The method for determining and calibrating the onset transformation temperatures for the different cooling/heating rates in DSC detection.

The intersection of the tangents to the heat flow trace (endothermic peak) is typically considered the onset transformation temperature for a sample, and this method was used to determine the onset temperatures of 1150 °C for Ti-42.5Al (Figure S1a) and 1146 °C for Ti-44Al (Figure S1b). However, this method does not guarantee the accuracy of those onset temperatures, whether the process is performed manually or automatically. Therefore, in this work, to improve the accuracy and uniformity of the data acquisition process, the first derivatives of the DSC traces (DDSC) [1] were employed to determine the transformation temperatures. As the maximum of the heat flow rate, the endothermic peak in the DDSC represents the maximum of the transformation's driving force in this condition. A given phase field (e.g., the α phase in the Ti-Al binary diagram) will be adjacent to a two-phase field with upper and lower transus temperatures, respectively. As the material is heated to the transformation temperature, a titanium aluminide with fixed components will undergo a transition in physical state and structural configuration, which requires extra energy as the driving force necessary to surpass the potential barrier. From this point of view, the maximum of the driving force, as the endothermic peak in the DDSC, could be rationally designated as the beginning of the transformation. Therefore, this work adopted the endothermic peak of the DDSC to indicate the transformation temperature, and this method was used to determine the onset temperatures of 1161 °C for Ti-42.5Al (Figure S1.a) and 1155 °C for Ti-44Al (Figure S1.b).

There are several advantages to using the DDSC endothermic peaks to identify transformation temperatures. First, this method is more rational than using the tangent intersection. The onset transformation temperature determined by DDSC indicates the maximum driving force during the state transition, which has the same physical meaning as supercooling (a cooling process). As shown in Figure S1, the endothermic component prior to the point of maximum driving force indicates the incubation period of the state transformation. After this maximum, the transformation may proceed automatically, corresponding to a decreased driving force. Second, the DDSC method supports greater accuracy and uniformity of the data and associated statistics, with fewer introduced errors.

Moreover, the heating/cooling rates have significant effects on the transformation temperatures [2-6]. Thus, the effects of heating/cooling rates on the transformation temperatures should be considered and calibrated prior to the entire determination process to achieve equilibrium data. The invariant points, defined as the points at which the eutectoid reaction ($\alpha \leftrightarrow \alpha_2+\gamma$) occurs, of the Ti-Al alloys were identified from the DSC measurements according to Appel et al. [7] and Malinov et al. [8].

The difference between the equilibrium transformation temperature (T_i) and the actually detected temperature (T_a) is commonly defined as the temperature difference (ΔT): $\Delta T = T_i - T_a$. As mentioned in Refs. [3-6,9], the equilibrium temperature can be determined by extrapolating transformation temperatures determined with different heating/cooling rates (R) using a linear regression. According to the studies of Bhambri et al. [2], as shown in Figure S1(c), the slopes of the extrapolation lines are linearly distributed for the Ti-Al-(4-8)Nb alloys, indicating that the slope (S) value is a constant. Thus, there is a geometrical relationship between S (in absolute value), R, and ΔT, which appears as $S = \Delta T/R$. That is, the calibration parameters for a dynamic detection, ΔT, can be defined by the equation: $\Delta T = S \times R$. Therefore, the temperature difference of a specific alloy, with a given heating/cooling rate (R), can be exactly determined, as $T_i = T_a - \Delta T = T_a - S \times R$.

In this work, the transformation temperatures of Ti-40.5Al-8Nb alloy (Sample S12) with heating rates of 1, 5, and 10 °C/min were detected, as shown in Figure S1(d). The slope, S, of the extrapolation line was approximately 3.8, indicating that the temperature difference, ΔT, was approximately 38 °C for R = 10 °C/min, as shown in Figure S1(d).

To verify the accuracy and reliability of this determination method and calibration parameter, the transformation temperatures of invariant points in Ti-Al binary alloys were determined. After calibration, the transformation temperatures of invariant points in Ti-42.5Al and Ti-44Al samples were determined to be 1123 °C and 1117 °C, respectively, which are in the vicinity of the temperatures determined in previous studies, 1114 °C [10] and 1120 °C [11]. These results indicated the appropriateness of the selected determination method and calibration parameters, and the temperature difference, ΔT=38 °C, was therefore adopted to calibrate the dynamic transformation temperatures. The onset transition temperatures of the samples after calibration are presented in Table S1. The DSC/DTA data for detecting the phase transition temperatures in the Ti-Al-Nb samples from the literatures are presented in Table S2 and S3.

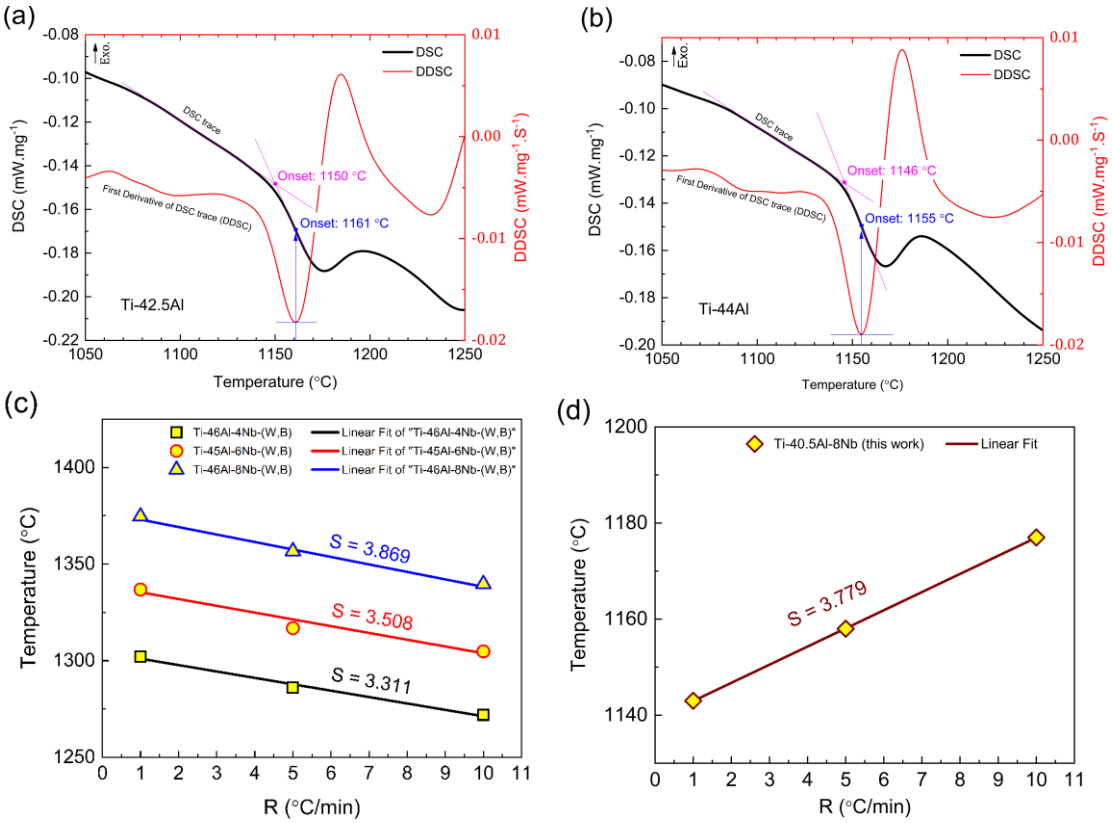

Figure S1. DSC and DDSC traces for samples that are closed to invariant points: (a) Ti-42.5Al and (b) Ti-44Al. Linear extrapolation of transformation temperatures of TiAl-based alloys: (c) Ti-(45-46)Al-(4-8)Nb-(W,B) [2] and (d) Ti-40.5Al-8Nb (this work).

Table S1. Onset phase transformation temperatures detected by thermal analysis.

Sample No.	Phase transformation temperatures (°C)						
S01	840	941	1183	---	---	---	---
S02	850	920	1109	1304	---	---	---
S03	840	976	1188	1328	---	---	---
S04	850	1056	1217	1352	---	---	---
S05	856	1149	1309	1369	---	---	---
S06	826	892	1183	1331	1373	---	---
S07	854	980	1184	1318	1365	---	---
S08	851	1186	1298	1343	1369		---
S09	852	881	1106	1181	1253	1301	1359
S10	824	850	880	1015	1177	1222	1341
S11	843	1151	1254	1302		---	---
S12	834	881	1138	1173	1265	1309	
S13	850	1149	1195	1312		---	---
S14	850	1148	1190	1243	1314	1392	
S15	1166	1239	1283	1361	---	---	---
S16	851	1161	1225	1291	1374	---	---
S17	956	1131	1245	1308	1352	1396	---
S18	1308	1354	---	---	---	---	---

Table S2. DSC/DTA data for detecting the phase transition temperatures in the Ti-Al-Nb samples from the literatures.

Nominal Comp. (at.%)	Phase Transition Temperatures (°C)					Ref.
	$\beta \leftrightarrow \beta_o$	$\alpha \leftrightarrow \beta$	$\alpha \leftrightarrow \gamma$	$\alpha \leftrightarrow \beta_o+\gamma$ & $\beta_o \leftrightarrow \alpha_2+\gamma$	$\beta_o \leftrightarrow \omega_o$	
Ti-42Al-8.5Nb	1200	1300	1238	1169	928	[6]
Ti-43.5Al-4Nb-1Mo-0.1B	1225	-	1247	1173	-	[5,12]
	-	-	1260	1115	-	[13]
	-	1405	1255	1160	-	[14]
Ti-43.5Al-4Nb-1.5Mo-0.1B	-	-	1246	1187	-	[5]
Ti-43.3Al-4.3Nb-1.2Mo-0.1B	1190	-	1265	1175	-	[15]
Ti-43.5Al-5Nb-1Mo-0.1B	-	-	1254	1180	-	[5]
Ti-45Al	-	-	1311	1122	-	[9]
Ti-45Al-5Nb	-	-	1295	1151	-	[9,16]
Ti-45Al-5Nb-0.5C	-	-	1295	1197	-	[16]
Ti-45Al-7.5Nb	-	-	1293	1159	-	[9,16]
Ti-45Al-7.5Nb-0.25C	-	-	1292	1180	-	[16]
Ti-45Al-7.5Nb-0.5C	-	-	1293	1200	-	[16]
Ti-45Al-7.5Nb-0.5C	-	-	1292	1203	-	[17]
Ti-45Al-8Nb	-	-	-	1170	-	[18]
Ti-45Al-10Nb	-	-	1299	1189	913	[9]
Ti-45Al-10Nb (cooling)	-	-	-	-	780	[3]
Ti-45Al-10Nb (heating)	-	-	-	-	870	[3]
Ti-46Al-9Nb	-	-	1330	1170	-	[19]
Ti-46Al-7Nb	-	1377	1327	1197	-	[20]
Ti-46Al-7Nb-2Mo	-	1427	1327	1197	-	[20]
Ti-46Al-7Nb-0.5C	-	1397	1307	1222	-	[20]
Ti-44Al-5Nb-3Cr-1.5Zr	-	1398	1320	1197	-	[21]

* The effect of heating/cooling rate on transition temperature is not concerned and calibrated in these data.

Table S3. Experimental transition temperatures in the Ti-Al-Nb samples summarized by Witusiewicz et al. [22]

Composition	Process	Phase Transition Temperatures (°C) *						
Ti-22.1Al-10.6Nb	Heating	911	1114	1695	1725	---	---	---
	Cooling	855	1145	1685	---	---	---	---
Ti-37Al-12.6Nb	Heating	820	945	1140	1230	1640	1675	---
	Cooling	1023	1198	1313	1488	1908	---	---
Ti-44.3Al-11.9Nb	Heating	1154	1228	1314	1390	1463	1547	1603
	Cooling	1145	1238	1401	1456	1541	1596	
Ti-44.9Al-8.2Nb	Heating	1163	1312	1393	1433	1471	1530	1593
	Cooling	1129	1151	1253	1378	1445	1517	1571
Ti-45.8Al-8.1Nb	Heating	1175	1352	1430	1479	1512	1586	---
	Cooling	1140	1284	1390	1472	1505	---	---
Ti-46.9Al-8.1Nb	Heating	1172	1362	1465	1493	1515	1568	---
	Cooling	1112	1182	1359	1440	1481	1499	1553
Ti-47.1Al-4.1Nb	Heating	1454	1626	1756	1778	1787	1824	---
	Cooling	1160	1342	1465	1491	1537	---	---
Ti-47.8Al-7.7Nb	Heating	1107	1234	1388	1490	1508	1530	---
	Cooling	1192	1349	1459	1486	1535	---	---
Ti-49.6Al-7.3Nb	Heating	1305	1424	1480	1514	1528	---	---
	Cooling	1212	1403	1452	1496	1511	---	---
Ti-54.1Al-7.6Nb	Heating	1455	1488	1498	---	---	---	---
	Cooling	1445	1458	1471	---	---	---	---

* The effect of heating/cooling rate on transition temperature is not concerned and calibrated in these data.

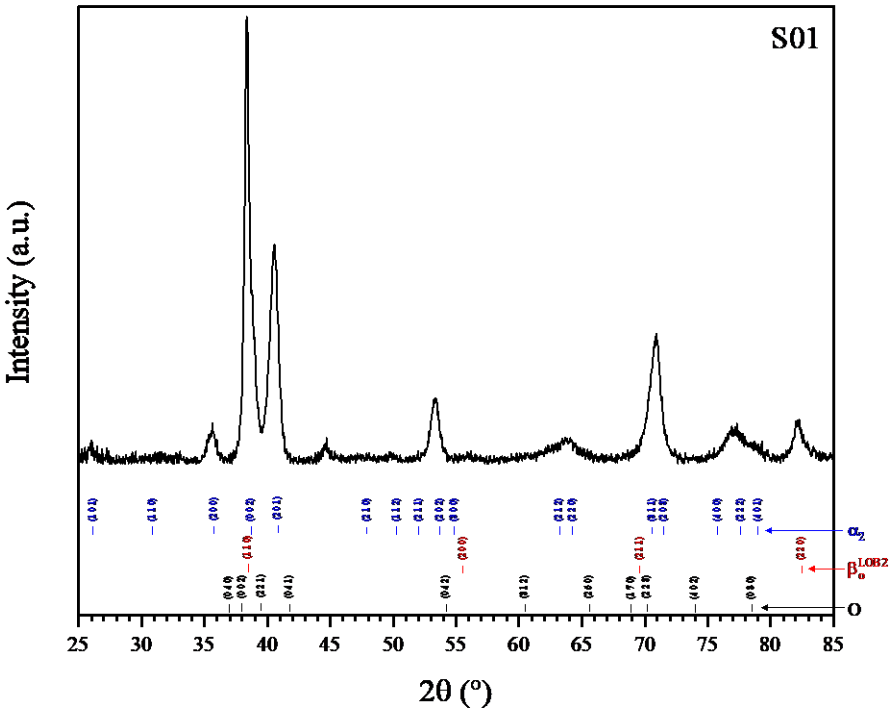
S01
Intensity (a.u.)
2θ (°)
25
30
35
40
45
50
55
60
65
70
75
80
85
α2
β°LOB2
O

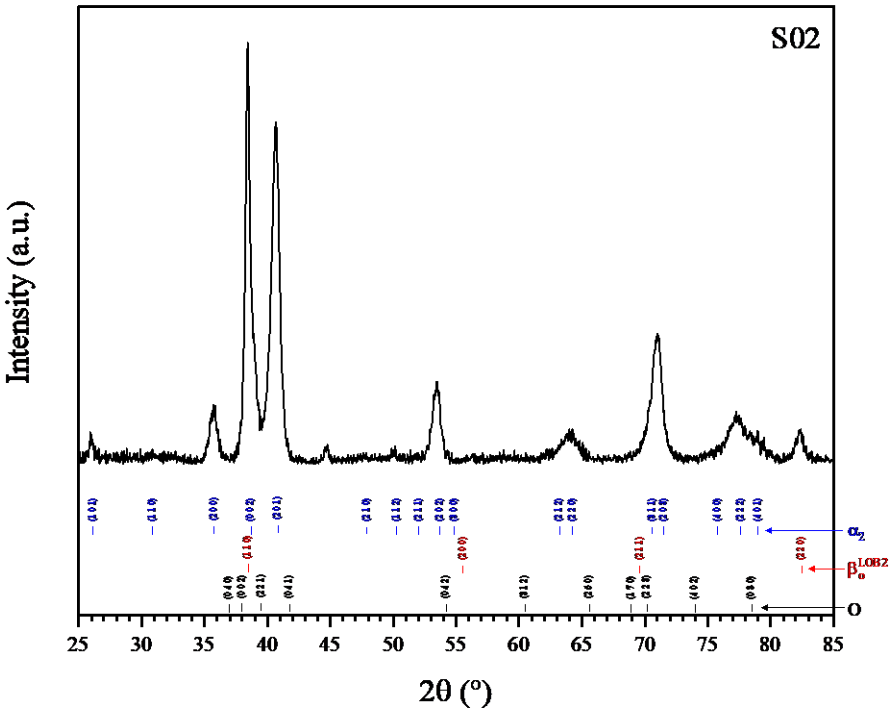
S02
Intensity (a.u.)
2θ (°)
25
30
35
40
45
50
55
60
65
70
75
80
85
α2
β°LOB2
O

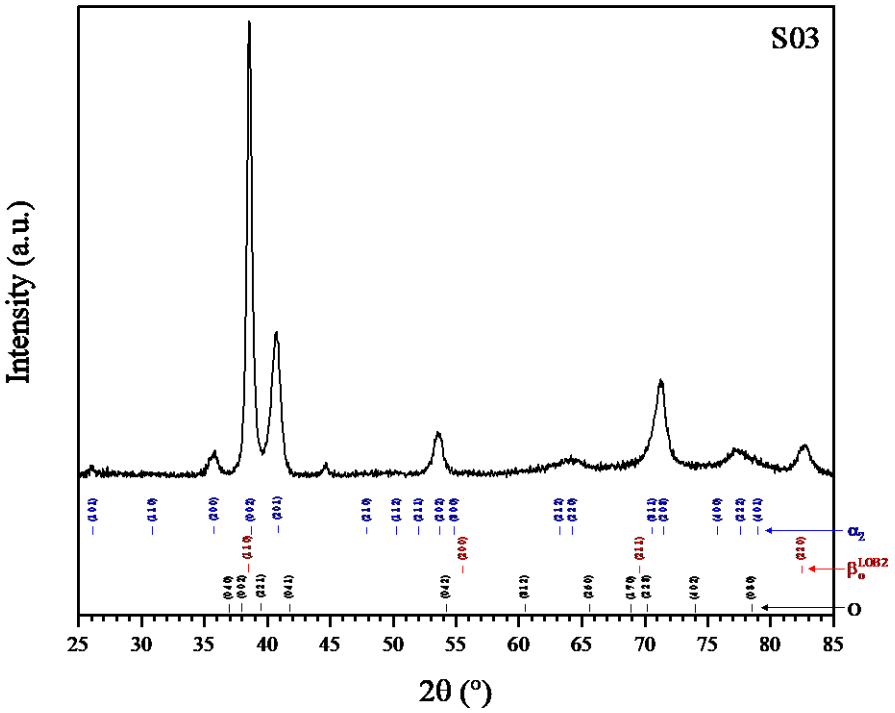
S03
Intensity (a.u.)
2θ (°)
25
30
35
40
45
50
55
60
65
70
75
80
85
α2
β'LOB2
O

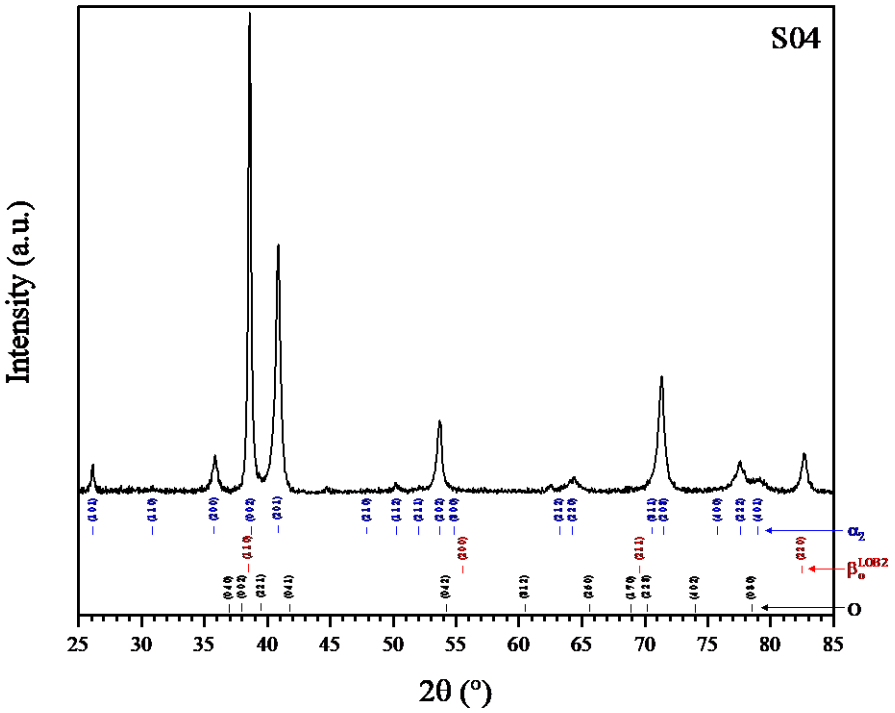
S04
Intensity (a.u.)
2θ (°)
25
30
35
40
45
50
55
60
65
70
75
80
85
α2
β'LOB2
O

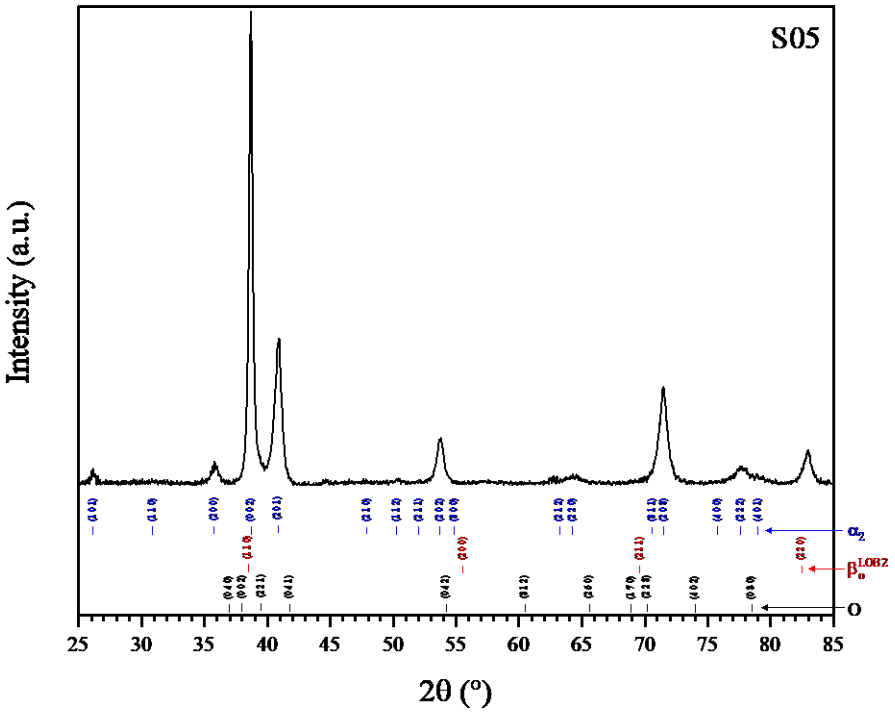
S05
Intensity (a.u.)
2θ (°)
25
30
35
40
45
50
55
60
65
70
75
80
85
α2
β'o LOB2
O

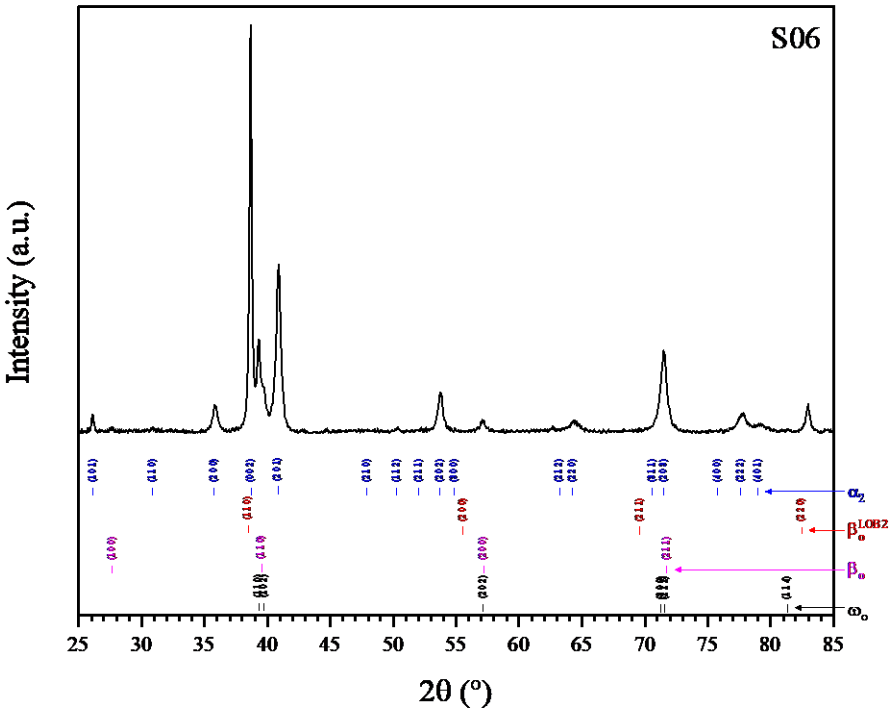
S06
Intensity (a.u.)
2θ (°)
25
30
35
40
45
50
55
60
65
70
75
80
85
α2
β'o LOB2
βo
ωo

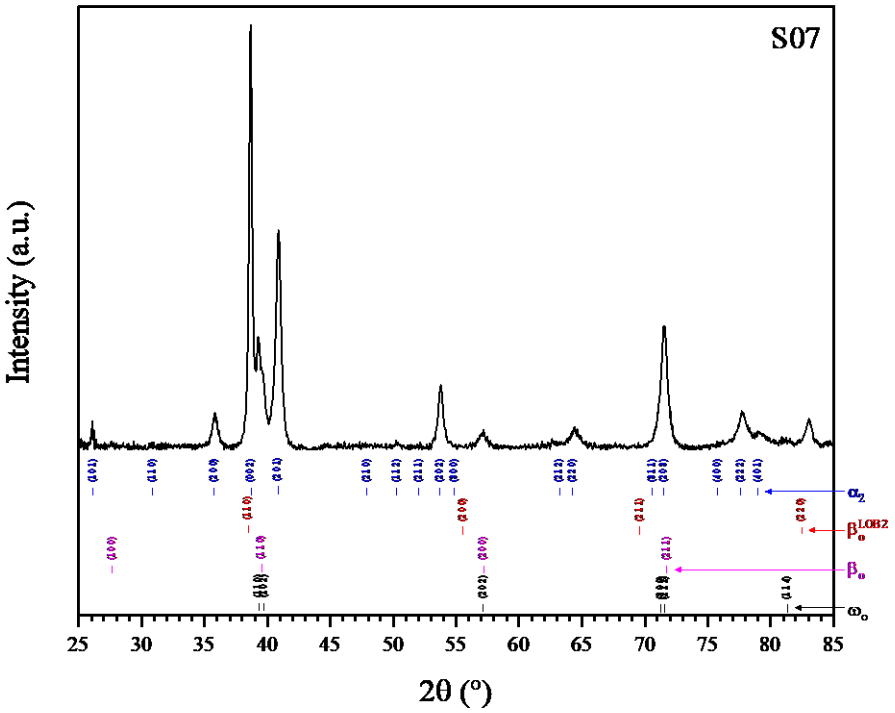
S07
Intensity (a.u.)
2θ (°)
25
30
35
40
45
50
55
60
65
70
75
80
85
α2
β0LOH2
β0
ω0

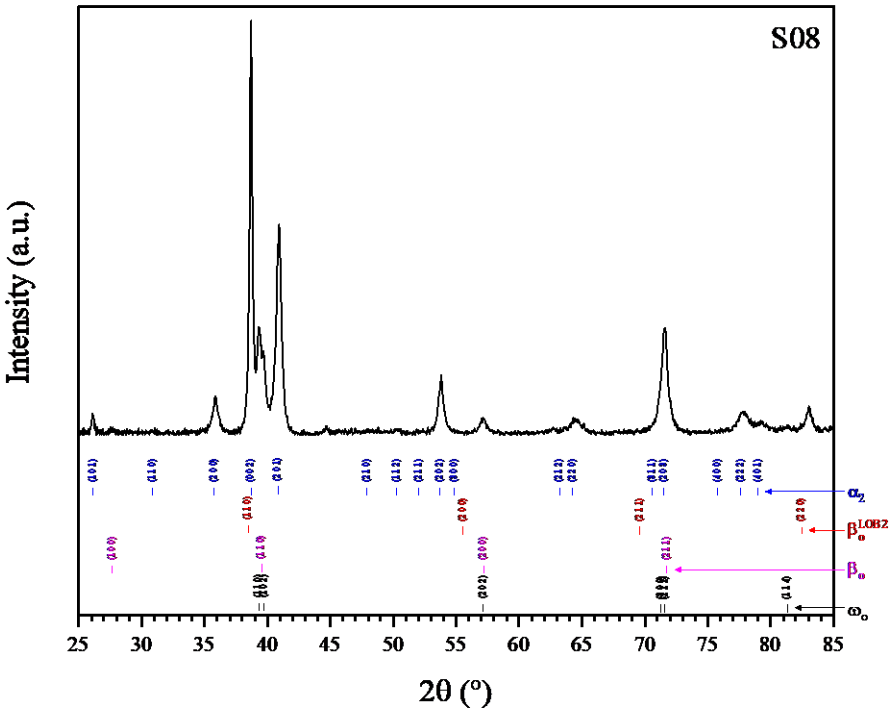
S08
Intensity (a.u.)
2θ (°)
25
30
35
40
45
50
55
60
65
70
75
80
85
α2
β0LOH2
β0
ω0

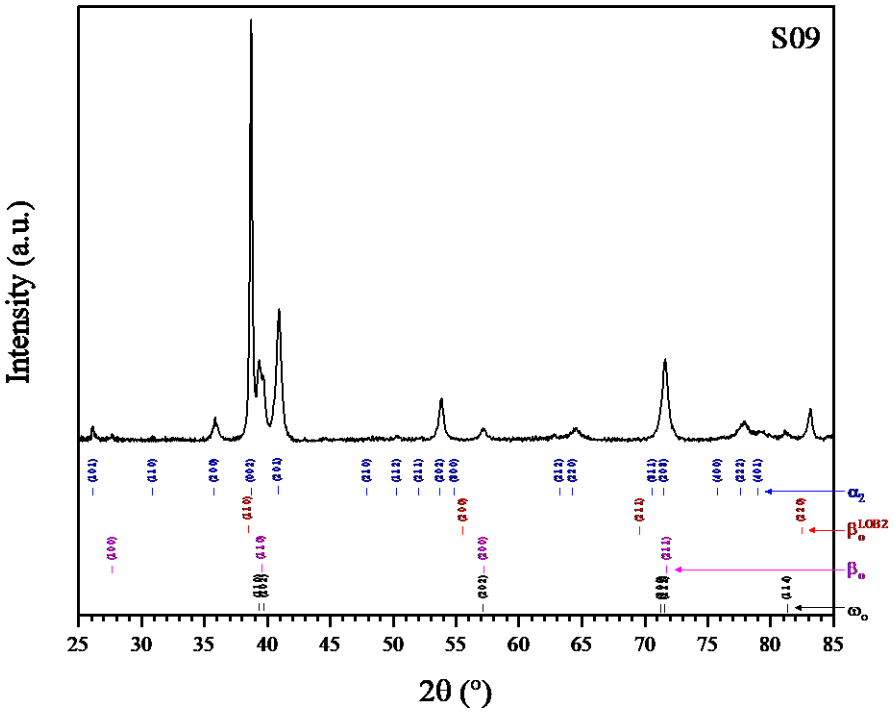
S09
Intensity (a.u.)
2θ (°)
25
30
35
40
45
50
55
60
65
70
75
80
85
α2
β0LOH2
β0
ω0

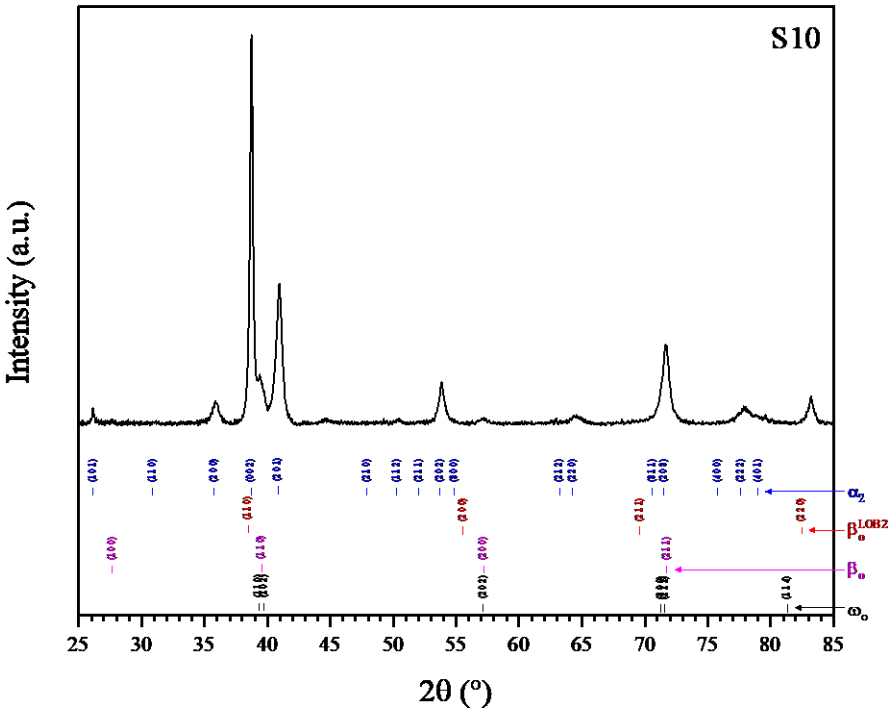
S10
Intensity (a.u.)
2θ (°)
25
30
35
40
45
50
55
60
65
70
75
80
85
α2
β0LOH2
β0
ω0

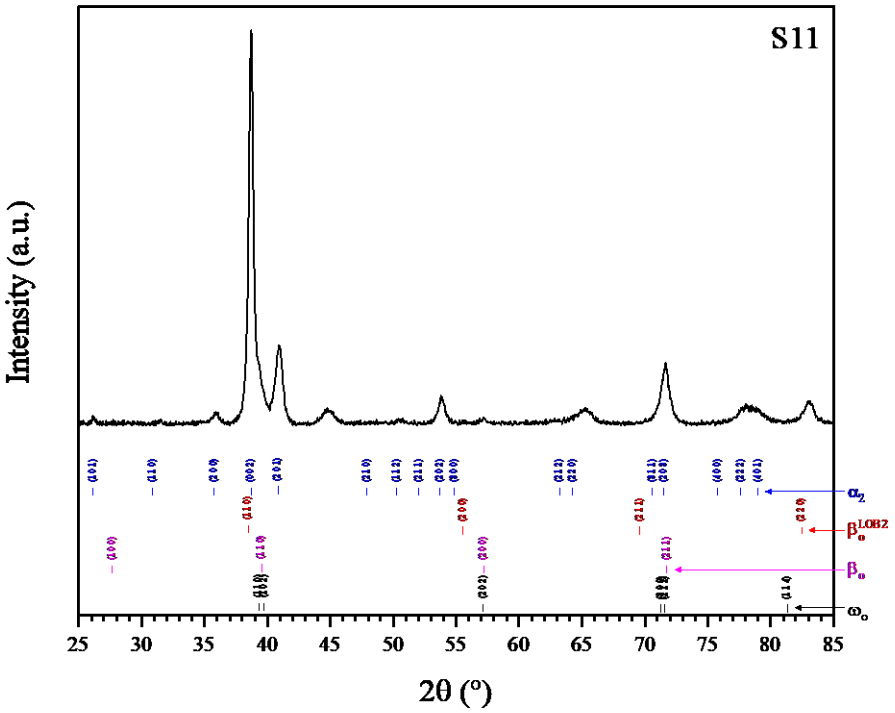
S11
Intensity (a.u.)
2θ (°)
25
30
35
40
45
50
55
60
65
70
75
80
85
α2
β0LOH2
β0
ω0

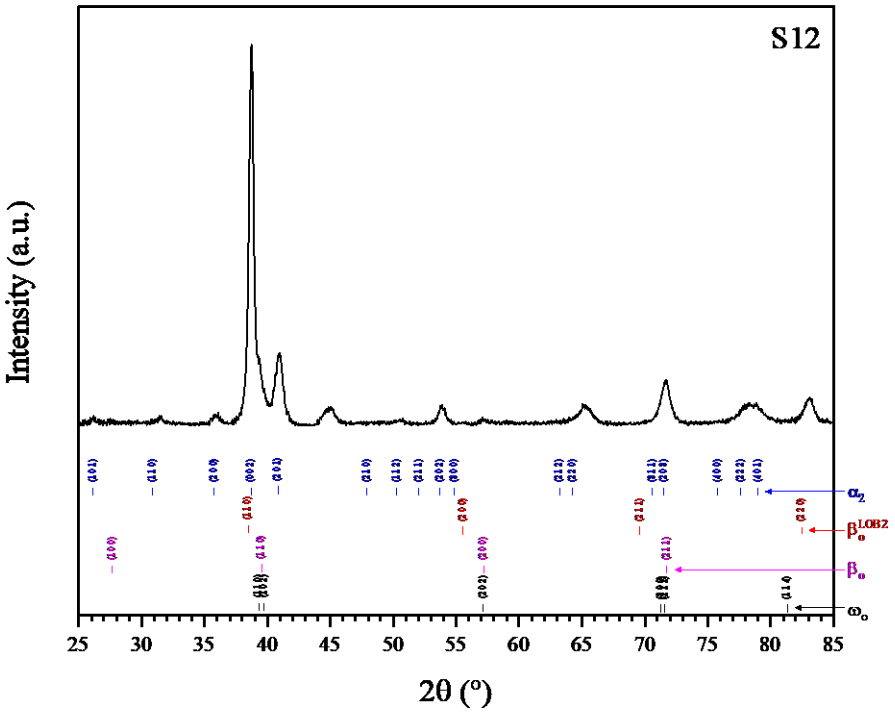
S12
Intensity (a.u.)
2θ (°)
25
30
35
40
45
50
55
60
65
70
75
80
85
α2
β0LOH2
β0
ω0

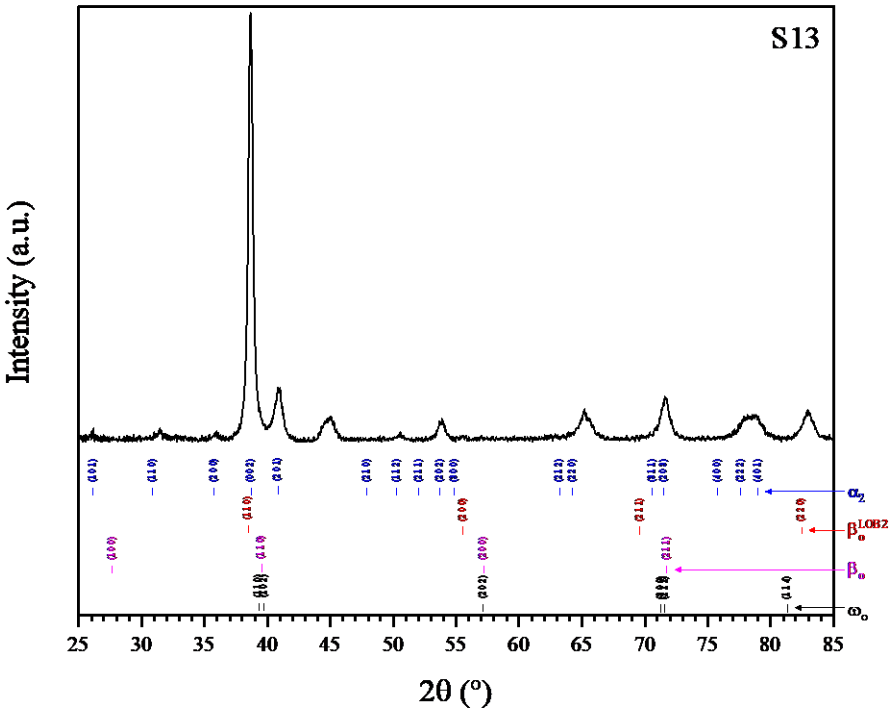
S13
Intensity (a.u.)
2θ (°)
25
30
35
40
45
50
55
60
65
70
75
80
85
α_2
β_o^{LOB2}
β_o
ω_o

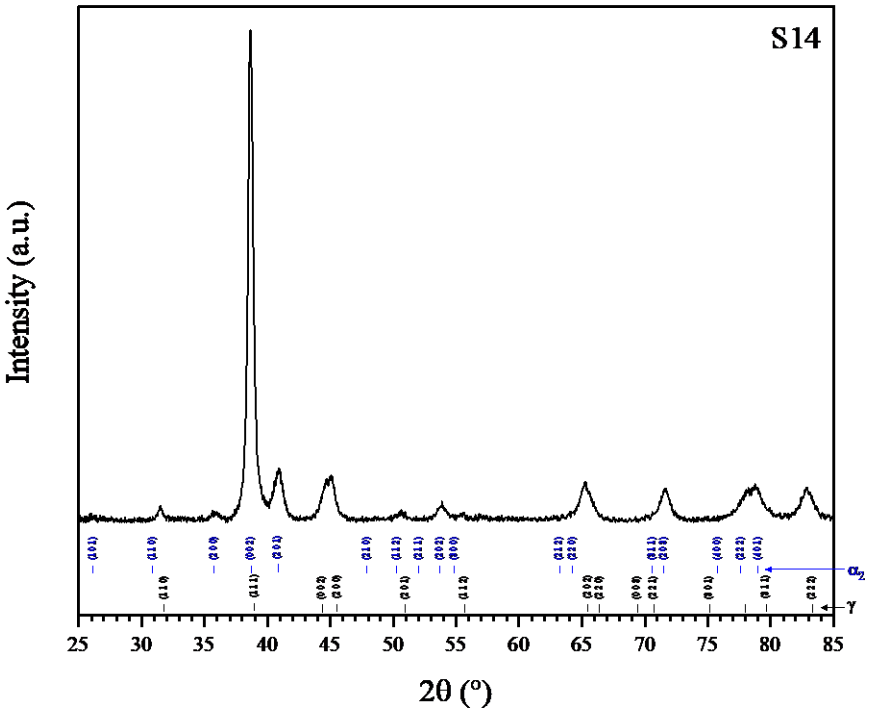
S14
Intensity (a.u.)
2θ (°)
25
30
35
40
45
50
55
60
65
70
75
80
85
α_2
γ

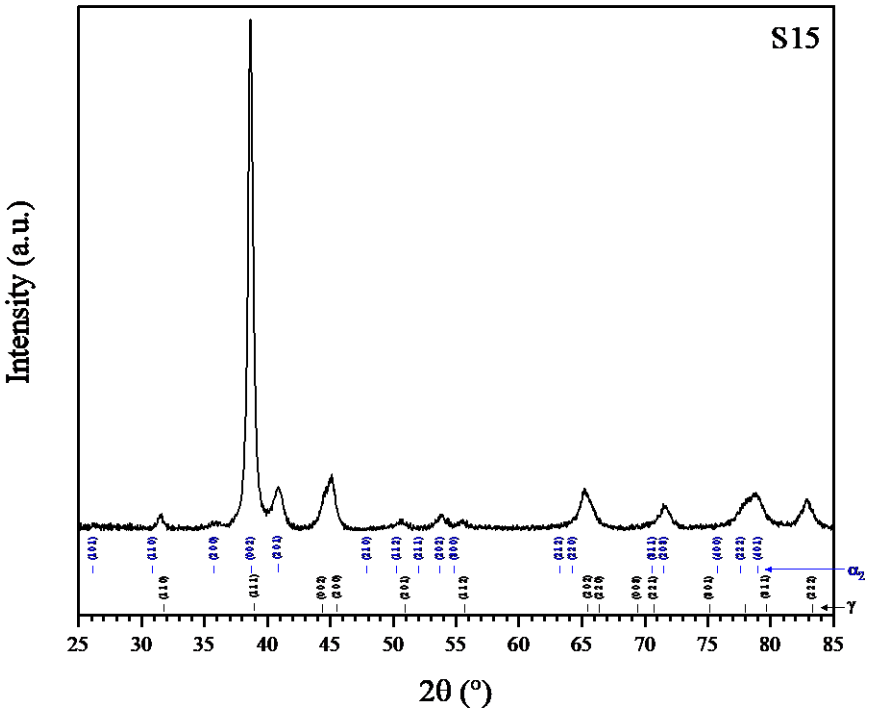
S15
Intensity (a.u.)
2θ (°)
25
30
35
40
45
50
55
60
65
70
75
80
85
α2
γ

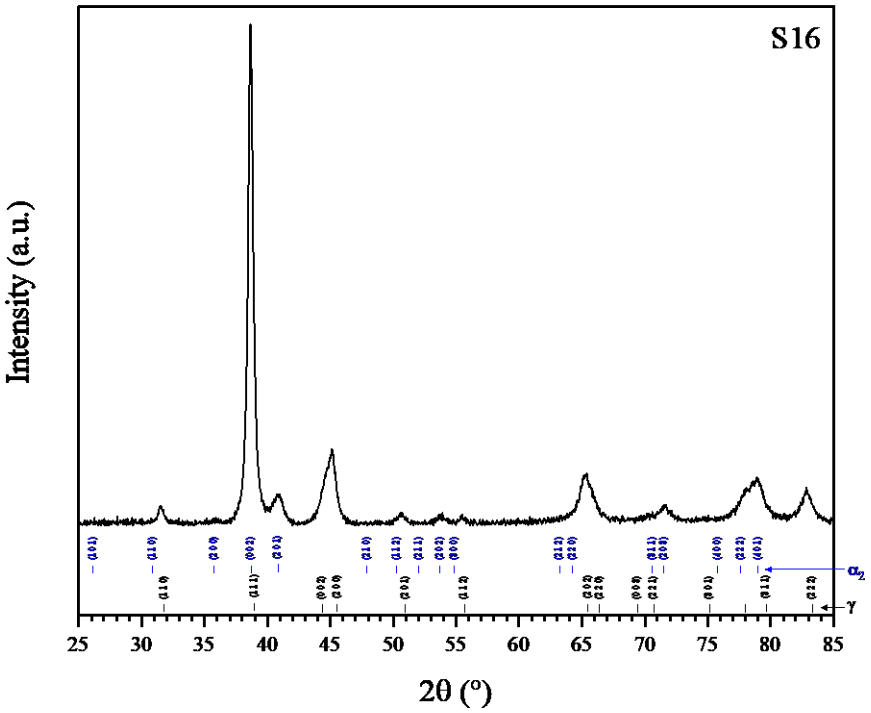
S16
Intensity (a.u.)
2θ (°)
25
30
35
40
45
50
55
60
65
70
75
80
85
α2
γ

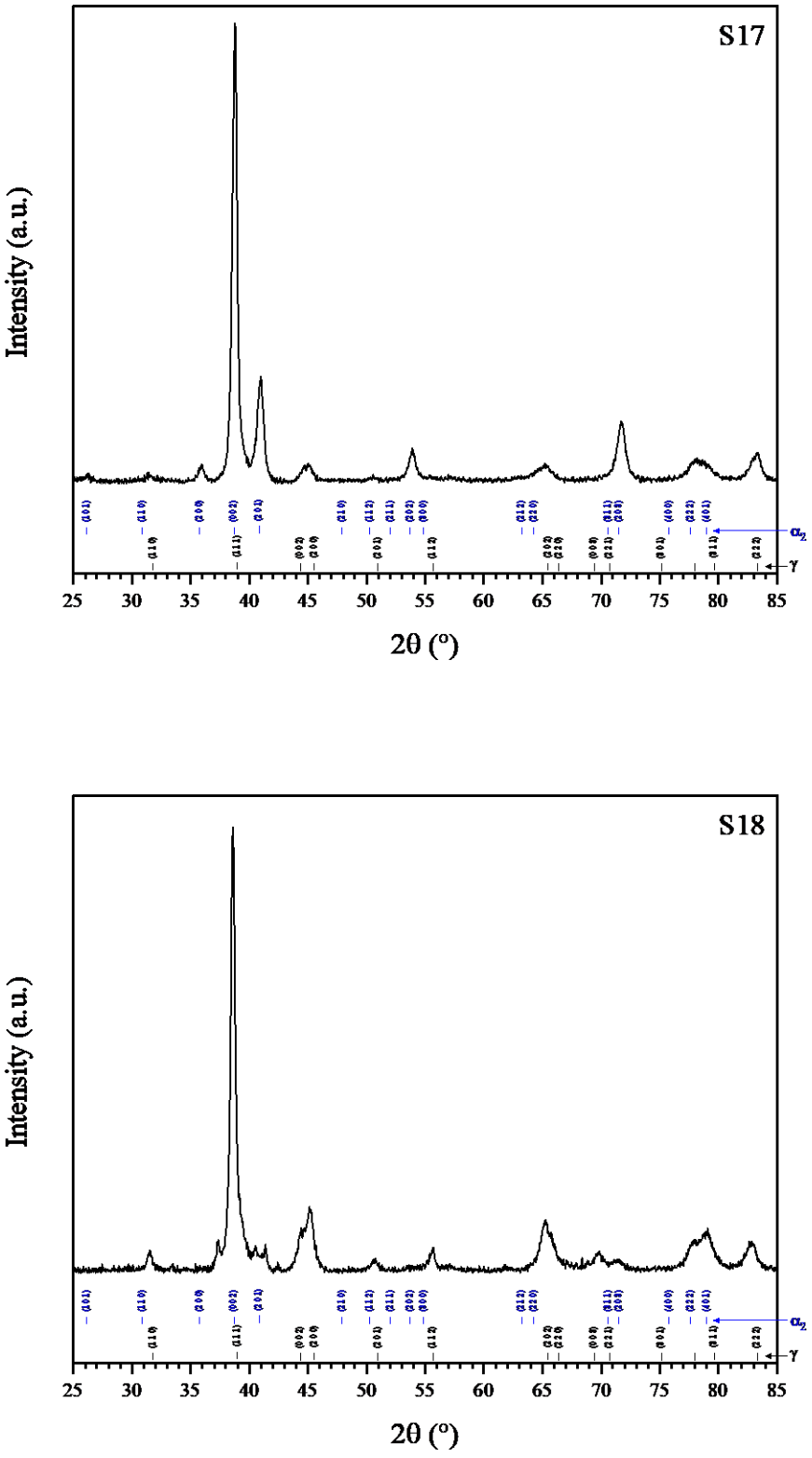

Figure S2. XRD patterns of S01-S18 samples, with relevant phase identification data.

References

1. Ilatovskaia, M.O.; Sinyova, S.I.; Starykh, R.V. Phase equilibria in the ternary Fe-Co-S system. *Calphad* **2017**, *59*, 31-39.
2. Bhambri, Y.; Sikka, V.K.; Porter, W.D.; Loria, E.A.; Carneiro, T. Effect of composition and cooling rate on the transformation of α to γ phase in TiAl alloys. *Materials Science and Engineering: A* **2006**, *424*, 361-365.
3. Stark, A.; Oehring, M.; Pyczak, F.; Schreyer, A. In Situ Observation of Various Phase Transformation Paths in Nb-Rich TiAl Alloys during Quenching with Different Rates. *Advanced Engineering Materials* **2011**, *13*, 700-704.
4. Schmoelzer, T.; Stark, A.; Schwaighofer, E.; Lippmann, T.; Mayer, S.; Clemens, H. In Situ Synchrotron Study of B19 Phase Formation in an Intermetallic γ-TiAl Alloy. *Advanced Engineering Materials* **2012**, *14*, 445-448.
5. Schmoelzer, T.; Liss, K.-D.; Zickler, G.A.; Watson, I.J.; Droessler, L.M.; Wallgram, W.; Buslaps, T.; Studer, A.; Clemens, H. Phase fractions, transition and ordering temperatures in TiAl–Nb–Mo alloys: An in- and ex-situ study. *Intermetallics* **2010**, *18*, 1544-1552.
6. Rackel, M.W.; Stark, A.; Gabrisch, H.; Schell, N.; Schreyer, A.; Pyczak, F. Orthorhombic phase formation in a Nb-rich γ-TiAl based alloy – An in situ synchrotron radiation investigation. *Acta Materialia* **2016**, *121*, 343-351.
7. Appel, F.; Oehring, M.; Wagner, R. Novel design concepts for gamma-base titanium aluminide alloys. *Intermetallics* **2000**, *8*, 1283-1312.
8. Malinov, S.; Novoselova, T.; Sha, W. Experimental and modelling studies of the thermodynamics and kinetics of phase and structural transformations in a gamma TiAl-based alloy. *Materials Science and Engineering: A* **2004**, *386*, 344-353.
9. Chladil, H.F.; Clemens, H.; Zickler, G.A.; Takeyama, M.; Kozeschnik, E.; Bartels, A.; Buslaps, T.; Gerling, R.; Kremmer, S.; Yeoh, L.; et al. Experimental studies and thermodynamic simulation of phase transformations in high Nb containing γ-TiAl based alloys. *International Journal of Materials Research* **2007**, *98*, 1131-1137.
10. Witusiewicz, V.T.; Bondar, A.A.; Hecht, U.; Rex, S.; Velikanova, T.Y. The Al-B-Nb-Ti system: III. Thermodynamic re-evaluation of the constituent binary system Al-Ti. *Journal of Alloys and Compounds* **2008**, *465*, 64-77.
11. Schuster, J.; Palm, M. Reassessment of the binary Aluminum-Titanium phase diagram. *Journal of Phase Equilibria and Diffusion* **2006**, *27*, 255-277.
12. Watson, I.J.; Liss, K.-D.; Clemens, H.; Wallgram, W.; Schmoelzer, T.; Hansen, T.C.; Reid, M. In Situ Characterization of a Nb and Mo Containing γ-TiAl Based Alloy Using Neutron Diffraction and High-Temperature Microscopy. *Advanced Engineering Materials* **2009**, *11*, 932-937.
13. Clemens, H.; Chladil, H.F.; Wallgram, W.; Zickler, G.A.; Gerling, R.; Liss, K.D.; Kremmer, S.; Güther, V.; Smarsly, W. In and ex situ investigations of the β-phase in a Nb and Mo containing γ-TiAl based alloy. *Intermetallics* **2008**, *16*, 827-833.

14. Schwaighofer, E.; Clemens, H.; Mayer, S.; Lindemann, J.; Klose, J.; Smarsly, W.; Güther, V. Microstructural design and mechanical properties of a cast and heat-treated intermetallic multi-phase γ-TiAl based alloy. *Intermetallics* **2014**, *44*, 128-140.
15. Erdely, P.; Werner, R.; Schwaighofer, E.; Clemens, H.; Mayer, S. In-situ study of the time–temperature-transformation behaviour of a multi-phase intermetallic β-stabilised TiAl alloy. *Intermetallics* **2015**, *57*, 17-24.
16. Chladil, H.F.; Clemens, H.; Leitner, H.; Bartels, A.; Gerling, R.; Schimansky, F.P.; Kremmer, S. Phase transformations in high niobium and carbon containing γ-TiAl based alloys. *Intermetallics* **2006**, *14*, 1194-1198.
17. Yeoh, L.A.; Liss, K.-D.; Bartels, A.; Chladil, H.; Avdeev, M.; Clemens, H.; Gerling, R.; Buslaps, T. In situ high-energy X-ray diffraction study and quantitative phase analysis in the α + γ phase field of titanium aluminides. *Scripta Materialia* **2007**, *57*, 1145-1148.
18. Chen, G.L.; Zhang, W.J.; Liu, Z.C.; Li, S.J.; Kim, Y.-W. Gamma Titanium Aluminides. In Proceedings of the TMS, Warrendale, PA, 1999; p. 371.
19. Liss, K.-D.; Bartels, A.; Clemens, H.; Bystrzanowski, S.; Stark, A.; Buslaps, T.; Schimansky, F.-P.; Gerling, R.; Scheu, C.; Schreyer, A. Recrystallization and phase transitions in a γ-TiAl-based alloy as observed by ex situ and in situ high-energy X-ray diffraction. *Acta Materialia* **2006**, *54*, 3721-3735.
20. Beran, P.; Petrenec, M.; Heczko, M.; Smetana, B.; Žaludová, M.; Šmíd, M.; Kruml, T.; Keller, L. In-situ neutron diffraction study of thermal phase stability in a γ-TiAl based alloy doped with Mo and/or C. *Intermetallics* **2014**, *54*, 28-38.
21. Kartavykh, A.V.; Asnis, E.A.; Piskun, N.V.; Statkevich, I.I.; Stepashkin, A.A.; Gorshenkov, M.V.; Akopyan, T.K. Complementary thermodynamic and dilatometric assessment of phase transformation pathway in new β-stabilized TiAl intermetallics. *Materials Letters* **2017**, *189*, 217-220.
22. Witusiewicz, V.T.; Bondar, A.A.; Hecht, U.; Velikanova, T.Y. The Al-B-Nb-Ti system: IV. Experimental study and thermodynamic re-evaluation of the binary Al-Nb and ternary Al-Nb-Ti systems. *Journal of Alloys and Compounds* **2009**, *472*, 133-161.